Fabrication of Large Area Ag Gas Diffusion Electrode via Electrodeposition for Electrochemical CO$_2$ Reduction

Seonhwa Oh [1], Hyanjoo Park [1], Hoyoung Kim [1], Young Sang Park [1,2], Min Gwan Ha [2], Jong Hyun Jang [2] and Soo-Kil Kim [1,*]

[1] School of Integrative Engineering, Chung-Ang University, Seoul 06974, Korea; iiioii2@naver.com (S.O.); hyanjoo89@gmail.com (H.P.); town57@naver.com (H.K.); bakyoungs@kist.re.kr (Y.S.P.)

[2] Center for Hydrogen Fuel Cell Research, Korea Institute of Science and Technology (KIST), Seoul 02792, Korea; jojaryoo@gmail.com (M.G.H.); jhjang@kist.re.kr (J.H.J.)

* Correspondence: sookilkim@cau.ac.kr; Tel.: +82-2-820-5770

Abstract: For the improvement for the commercialization of electrochemical carbon dioxide (CO$_2$) conversion technology, it is important to develop a large area Ag gas diffusion electrode (GDE), that exhibits a high electrochemical CO$_2$ conversion efficiency and high cell performance in a membrane electrode assembly (MEA)-type CO$_2$ electrolyzer. In this study, the electrodeposition of Ag on a carbon-paper gas diffusion layer was performed to fabricate a large area (25.5 and 136 cm^2) Ag GDE for application to an MEA-type CO$_2$ electrolyzer. To achieve uniformity throughout this large area, an optimization of the electrodeposition variables, such as the electrodes system, electrodes arrangement, deposition current and deposition time was performed with respect to the total electrolysis current, CO production current, Faradaic efficiency (FE), and deposition morphology. The optimal conditions, that is, galvanostatic deposition at 0.83 mA/cm^2 for 50 min in a horizontal, two-electrode system with a working-counter electrode distance of 4 cm, did ensure a uniform performance throughout the electrode. The position-averaged CO current densities of 2.72 and 2.76 mA/cm^2 and FEs of 83.78% (with a variation of 3.25%) and 82.78% (with a variation of 8.68%) were obtained for 25.5 and 136 cm^2 Ag GDEs, respectively. The fabricated 136 cm^2 Ag GDE was further used in MEA-type CO$_2$ electrolyzers having an active geometric area of 107.44 cm^2, giving potential-dependent CO conversion efficiencies of 41.99%–57.75% at V_{cell} = 2.2–2.6 V.

Keywords: carbon dioxide; Ag catalyst; gas diffusion electrode; electrodeposition

1. Introduction

Carbon dioxide (CO$_2$) is one of the representative greenhouse gases generated during the combustion and chemical processes of fossil fuels. Studies have been performed on the conversion of CO$_2$ into value-added chemicals via thermochemical, electrochemical and photochemical methods [1–6]. Among them, the electrochemical conversion of CO$_2$ is an effective way to generate various organic materials from CO$_2$ under atmospheric temperature and pressure conditions [7] by using product-selective catalysts and a liquid-dissolved/direct gaseous CO$_2$ feed. However, because CO$_2$ is thermodynamically stable, having a linear molecular structure, the use of a suitable catalyst is necessary to reduce CO$_2$. Depending on the selectivity of the catalyst, the products of electrochemical CO$_2$ conversion can vary, e.g., CO [8,9], CH$_4$ [10,11], C$_2$H$_6$ [12,13], HCOOH [14,15], and many other low-C products. Among the products, CO has the following benefits: a small amount of electrical energy required for production [16,17], a simple reaction path [18], and a high market price as a feed material for the Fischer–Tropsch process [19].

Thus, numerous studies have been performed on the electrochemical reduction of CO_2 to CO. Metal catalysts such as Au and Ag have high CO selectivity [7], since Au and Ag are known to have weak metal-CO binding [20] which is beneficial to CO production [21]. Although Ag has benefits over Au with regard to cost, it requires a higher overpotential than Au, owing to its moderate activity [22]. To overcome this, the fabrication of nanoparticles with unique shapes, such as nano-corals or triangular nanoplates, which maximize the amounts of active sites for CO production, has been attempted in many studies [23–25]. For example, Ag nano-coral catalysts fabricated by Hsieh et al. [23] had a CO production current density of 6.62 mA/cm^2, which was approximately 16.55 times higher than that of Ag nanoparticles.

However, most previous studies focused on the development of new catalysts having the advantageous physicochemical properties and high selectivity/activity for CO production at the laboratory level using half-cells and H-type cells [24,26–29], which cannot yet be scaled for commercialization. For the large-scale conversion of CO_2, systems using an aqueous solution-based electrolyte with dissolved CO_2 should be avoided, owing to the limited solubility of CO_2 in water (~0.03 mol kg^{-1} at ~300 K and 1 atm) [30]. In contrast, flow cell systems such as proton-exchange membrane (PEM)-based membrane electrode assembly (MEA)-type CO_2 electrolyzers [31–35], are capable of converting large amounts of CO_2. Some of them have achieved very high efficiencies of 80%–85%, with high CO partial current densities of 50–290 mA/cm^2 [31,33], and there are still items to consider, such as using commercial electrodes [31,32], a small electrode area [33,34], and high operating cell voltage [31]. In our previous study, we examined the performance of an Ag gas diffusion electrode (GDE), having a geometric area of 2.8×2.8 cm^2, and fabricated via electrodeposition to control hydrophilicity using acid-treated carbon paper for a PEM-based MEA-type CO_2 electrolyzer [36]. The PEM-based MEA-type CO_2 electrolyzer using Ag GDE is commercially advantageous, but in order to manufacture a high-capacity system for the large-scale conversion of CO_2, a fabrication method for large area electrodes must be developed.

In the present study, we present the studies of a large area (25.5 and 136 cm^2) Ag GDE, having a uniformly high electrochemical CO_2 conversion efficiency and high cell performance throughout the geometric area, which is suitable for scaling the MEA-type CO_2 electrolyzer. The main objective was to achieve the uniformity of the electrodeposited Ag catalyst over a large area for maintaining high activity, even with a large electrode. To achieve the effective production of large area electrodes using electrodeposition, the process variables that can affect the current distribution [37–39], such as the electrodes system, electrodes placement, deposition current density and deposition time, were optimized with regard to uniformity and performance.

2. Materials and Methods

2.1. Materials and Equipments

Ag catalysts were prepared via electrodeposition using a potentiostat (CS310, Wuhan CorrTest Instruments Corp., Ltd., Wuhan, China). The substrate for Ag electrodeposition was a carbon paper (AvCarb Material Solutions, Lowell, MA, USA; AvCarb MGL 280, 1594009)-based gas diffusion layer. The substrate was employed after pretreatment in a sulfuric acid (H_2SO_4; 95%, Junsei, 83010S1250) solution using a sonicator for 15 min [36]. A mixture of 0.6 M ammonium sulfate (($NH_4)_2SO_4$, 99%, 11566; Alfa Aesar, Haverhill, MA, USA) as the supporting electrolyte, 0.01 M silver nitrate ($AgNO_3$, 99.9%, Alfa Aesar, 11414) as the Ag precursor, and 0.04 M ethylenediamine ($C_2H_8N_2$, 99%, E1521; Aldrich, St. Louis, MO, USA) [40] was used as the electrolyte (pH of 8.6). The geometric area of the carbon paper used for electrodeposition was 25.5 and 136 cm^2, respectively, and the lead wires were connected either at the top or at the sides of the carbon paper according to the arrangement of the electrodes (Figure 1).

2.2. Fabrication of Ag GDE

The Ag catalyst was fabricated in both three-electrode and two-electrode systems to examine the differences in the morphology and CO_2 conversion efficiency, at room temperature and ambient pressure. For the three-electrode system, an electrodeposition of the Ag catalyst was performed using acid-treated carbon paper, a Pt plate, and a saturated calomel electrode (SCE, saturated KCl) as the working, counter, and reference electrodes, respectively, at −0.49 V (vs. SCE) for 50 min. The effect of the deposition time on the characteristics of the Ag catalysts can be found in our previous work, particularly on the adhesion problem at the longer deposition time [41]. For the two-electrode system, electrodeposition of the Ag catalyst was performed via galvanostatic methods for the same duration. The same working and counter electrodes were used: acid-treated carbon paper and a Pt plate, respectively. The galvanostatic deposition conditions were varied, such as the deposition current (0.63, 0.83 and 1.03 mA/cm^2), the distance between the working and counter electrodes (1, 2, 4 and 5 cm), and the deposition time (5 and 50 min). The morphology and uniformity of the Ag deposits were analyzed using field-emission scanning electron microscopy (FE-SEM, SIGMA, Carl Zeiss) at different positions on the large area Ag GDE (denoted as A–E). The loading amounts of Ag by electrodeposition were analyzed with inductively coupled plasma optical emission spectroscopy (ICPOES, Optima 8300, Perkin Elmer, Waltham, MA, USA).

2.3. Electrochemical CO_2 Reduction to CO in Half-Cell

For testing the CO_2 reduction to confirm the uniform activity throughout the large area Ag GDE, the electrodeposited Ag GDEs were cut into three pieces (for the 25.5 cm^2 GDE) or five pieces (for the 136 cm^2 GDE), each having a geometric area of 2.56 cm^2. The positions of the cut pieces are shown in Figure 1a,b and Figure 9a. Using the cut pieces as working electrodes, the electrochemical CO_2 reduction was conducted using a potentiostat (WaveNow, Pine Instrument, Grove City, PA, USA) in a laboratory-made H-type cell, where the cathodic and anodic parts were divided by a PEM (Nafion 212, Dupont^{TM}), and Pt gauze and an SCE were used as the counter and reference electrodes, respectively. The electrolyte and operating conditions for the CO_2 reduction were based on our previous experimental method [42]. In detail, 0.5 M potassium hydrogen carbonate (KHCO$_3$, 99.5%, 6580-4400, DaeJung, Siheung-si, South Korea) was used for both the anolyte and the catholyte. The catholyte was saturated with CO_2 gas for at least 30 min, and the anolyte was saturated with Ar gas for at least 30 min. During the operation, CO_2 gas was continuously injected into the catholyte at a flow rate of 10 mL/min using a flow controller to maintain the CO_2 saturation state. The CO_2 reduction was performed for 30 min under a constant voltage of −1.5 V (vs. SCE), and the generated gas (CO, H$_2$) was injected into a gas chromatograph (GC, 7890A, off-line mode, Agilent, Santa Clara, CA, USA). The produced H$_2$ and CO were detected using a thermal-conductivity detector and a flame ionization detector, respectively. The average electrolysis current density measured during the last 1 min of the reduction was denoted as the total current density. The electrochemical Faradaic efficiency (FE) and the CO production partial current [22] were calculated using the detected concentrations of CO and H$_2$, and the amounts of charge supplied during the same period of the last 1 min.
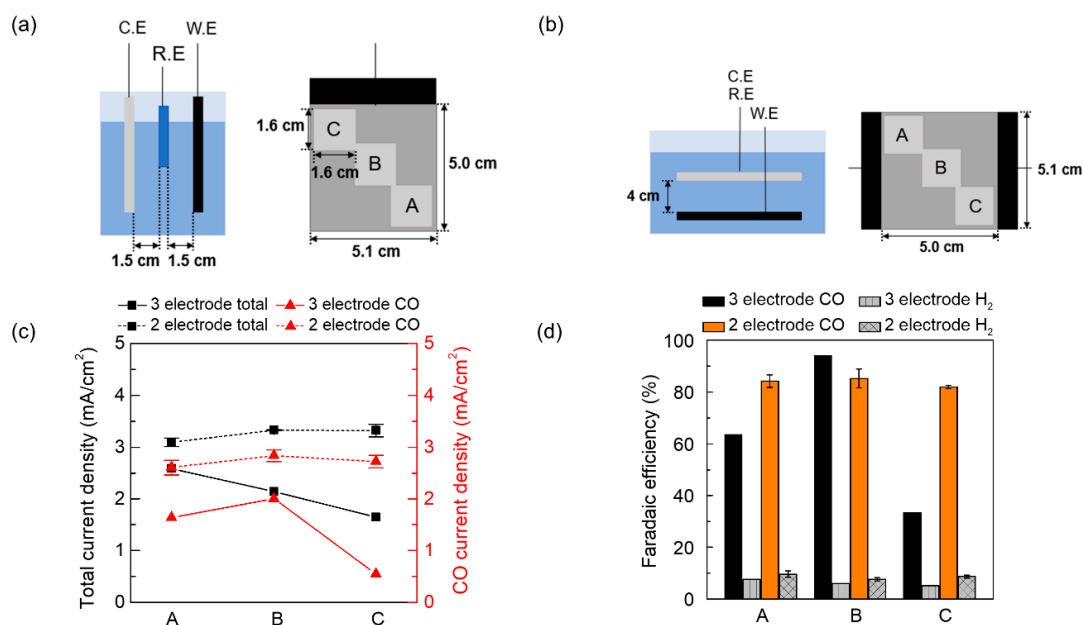
Figure 1. Schematic diagrams of the (**a**) vertical three-electrode system and (**b**) horizontal two-electrode system for fabricating the 25.5 cm^2 Ag gas diffusion electrode (GDE). The sectioned positions used in the subsequent analysis were denoted as A, B and C. (**c**) Total electrolysis current density and CO production current density of the Ag GDE fabricated in each electrode system according to the position and (**d**) the corresponding FE for CO and H$_2$. The Ag deposition conditions were −0.49 V (vs. the saturated calomel electrode (SCE)) for 50 min in the three-electrode system, and 0.83 mA/cm^2 for 50 min in the two-electrode system. The CO$_2$ reduction was performed at a constant voltage of −1.5 V (vs. SCE) in a laboratory-made H-type cell. 0.5 M KHCO$_3$ was used for both the anolyte and the catholyte.

2.4. Electrochemical CO$_2$ Reduction to CO in MEA-Type Electrolyzer

For the MEA-type CO$_2$ electrolyzer, the fabricated 136 cm^2 Ag GDE (actual geometric area of 107.44 cm^2) with the optimized electrodeposition condition was used as the working electrode. The counter electrode for oxygen evolution was fabricated by the spray coating of IrO$_2$ stock solution composed of IrO$_2$ (99.99%, Alfa Aesar), Nafion-perfluorinated resin binder (5 wt%, Sigma-Aldrich), isopropyl alcohol (70%, Honeywell Research Chemicals) and de-ionized water onto the oxalic-acid-pretreated Ti paper, giving 1 mg/cm^2 of IrO$_2$ loading. Once the electrodes were prepared, the MEA was fabricated by assembling the two electrodes with the PEM (Nafion 117, DuPont^{TM}). A thicker membrane of Nafion 117 (183 μm) was used in making MEA instead of Nafion 212 (50.8 μm) to ensure the mechanical stability under the condition of massive CO$_2$ feed and pressurized system explained in the forthcoming section.

10 mL/min of KHCO$_3$ solution (1.0 M; 99.7%, Sigma-Aldrich) and 100 mL/min of KOH solution (1.0 M; 90%, Sigma-Aldrich) were fed and circulated as the catholyte and anolyte, respectively, using flow fields at both electrodes. Gaseous CO$_2$ at a rate of 150 mL/min (the ratio of the volumetric gaseous flow rate to the cross-sectional area for the gas flow channel was 83.3 cm/sec) were also fed to the cathode using a separated flow field. The electrolysis performance was evaluated at a different cell potential (V_{cell}) range (1.8 to 3.4 V), using a potentiostat (HCP-803, Bio-Logic Science Instruments, Seyssinet-Pariset, France) under pressurized conditions at 4 bar. The amounts of produced CO and H$_2$ during the electrolysis were measured by a GC (7890B, Agilent, off-line mode).

3. Results and Discussion

Large area (25.5 cm^2) Ag GDEs were manufactured using three- and two-electrode systems to examine the effects of the electrode system on the uniformity of the catalyst formation and the

electrochemical CO_2 reduction efficiency. Figure 1a shows a schematic of the three-electrode system consisting of working, counter and reference electrodes. The reference electrode was between the working and counter electrodes, and the distance between the electrodes was maintained at 1.5 cm (Note that the placement of the reference electrode at the side of the working electrode was not adopted here, since it may cause severe non-uniform distribution in the solution resistances between the closest and the farthest parts of the working electrode, particularly in the case of the large area working electrode). Figure 1b shows a schematic of the two-electrode system consisting of working and counter electrodes, where the distance between the electrodes was fixed as 4 cm. Because there was no reference electrode in the two-electrode system, the reduced restriction on placing the electrodes allowed for a horizontal arrangement of the electrodes. In both figures, A, B and C represent the pieces cut to evaluate the uniformity within the electrode. The electrochemical CO_2 reduction using each piece in Figure 1a,b was measured. Both the total reduction current and the CO production partial current are presented in Figure 1c. As shown, the Ag GDE deposited via the two-electrode system exhibited higher total current density and CO current density values than the Ag GDE deposited via the three-electrode system. In particular, the Ag GDE fabricated via the two-electrode system exhibited similar total current density values (3.09–3.33 mA/cm^2) and CO current density values (2.61–2.83 mA/cm^2), regardless of the position within the large electrode. However, for the three-electrode system, the total current density was in the range of 1.65–2.58 mA/cm^2 according to the position, exhibiting non-uniformity. The non-uniformity was also severe in the case of the CO current density, which ranged from 0.55 to 2.01 mA/cm^2. The variation in the performance according to the position within the electrode was confirmed by examining the FE, as shown in Figure 1d. The Ag GDE fabricated via the two-electrode system exhibited a highly uniform and high CO FE of 81.95%–85.2%, regardless of the position. In contrast, the Ag catalyst fabricated via the three-electrode system exhibited a CO FE ranging from 33.5% to 93.88%, depending on the position, exhibiting severe non-uniformity. The non-uniform characteristics of the Ag GDE fabricated with the three-electrode system are attributed to the uneven mass transport caused by the insertion of the reference electrode between the working and counter electrodes. Moreover, the differences in the length from the reference electrode to each position of the large working electrode might have caused differences in the ohmic voltage drop.

This is supported by the morphologies of the deposited Ag, which are shown in Figure 2 for both electrode systems. Figure 2a shows the FE-SEM results for the Ag GDE deposited in the three-electrode system, and Figure 2b shows those for the two-electrode system, according to the position. In Figure 2a, a decrease in the deposition amount of the Ag catalyst from bottom to top (A → C) is observed. However, in Figure 2b, the deposition amount and morphology do not exhibit any significant differences with respect to the position. Therefore, with the two-electrode system, the electrodeposition of Ag exhibited higher uniformity throughout the electrode, which is important for the scale-up of the electrode. Therefore, electrodeposition using the two-electrode system was studied for the optimization of the deposition variables for fabrication of a 25.5 cm^2 large area GDE.

Figure 3 shows the total and CO partial current densities and the calculated FE, according to the position on the 25.5 cm^2 Ag GDE fabricated at different deposition currents of 0.63, 0.83 and 1.03 mA/cm^2 for the two-electrode system. The distance between the electrodes and the deposition time were fixed at 4 cm and 50 min, respectively. Regardless of the deposition current density, the Ag catalyst fabricated via the two-electrode system maintained uniformity in both the total and CO currents. The CO current densities at different positions were 2.25–2.51 mA/cm^2 for the deposition current density of 0.63 mA/cm^2, 2.61–2.83 mA/cm^2 for the deposition current density of 0.83 mA/cm^2, and 2.41–2.79 mA/cm^2 for the deposition current density of 1.03 mA/cm^2. Generally, the CO current density was highest when the Ag catalyst was deposited at 0.83 mA/cm^2. Figure 3b shows the FE of CO and H_2 according to the deposition current and position. For the deposition currents of 0.63, 0.83 and 1.03 mA/cm^2, the CO FE at different positions was 82.15%–85.5% (3.35% difference), 81.95%–85.2% (3.25% difference), and 77.65%–86.95% (9.3% difference), respectively. The 25.5 cm^2 large area Ag GDE fabricated via the two-electrode system with a deposition current of 0.83 mA/cm^2 had a high

CO current density and uniform CO FE of >80%. The morphologies of the Ag GDE according to the deposition current and position are presented in Figure 4. As shown, there was no significant difference in the morphologies of the Ag deposits, and Ag catalysts with a dendrite morphology were uniformly formed for all samples regardless of the deposition current density and the position.
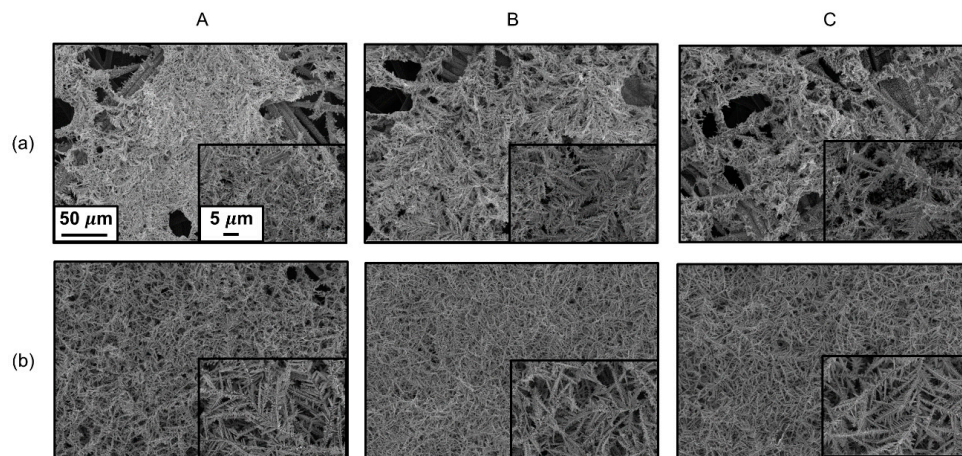

Figure 2. Field emission scanning electron microscope (FE-SEM) images of the fabricated 25.5 cm^2 Ag GDE (Figure 1) according to the position on the electrode: (**a**) three-electrode system; (**b**) two-electrode system.
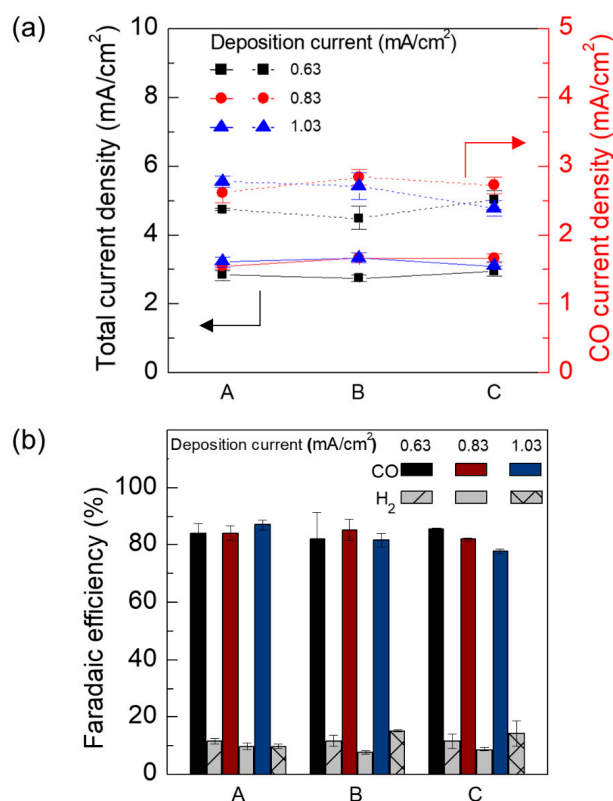
Figure 3. (**a**) Total electrolysis current density and CO production current density of the 25.5 cm^2 Ag GDE according to the position and (**b**) the corresponding FE for CO and H$_2$. Ag deposition was performed with different deposition current densities (0.63, 0.83 and 1.03 mA/cm^2) for 50 min with a fixed working-counter electrode distance of 4 cm. The CO$_2$ reduction was performed at a constant voltage of −1.5 V (vs. SCE) in a laboratory-made H-type cell. 0.5 M KHCO$_3$ was used for both the anolyte and the catholyte.
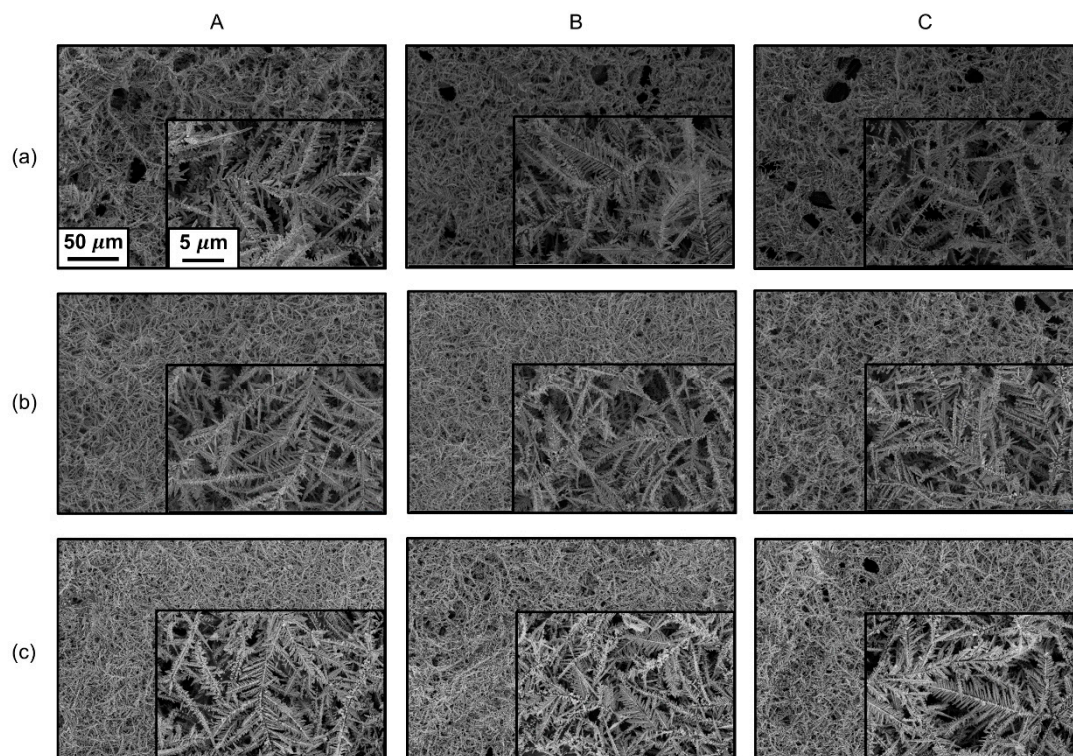
Figure 4. FE-SEM images of the fabricated 25.5 cm^2 Ag GDE (Figure 3) according to the position on the electrode. Ag deposition was performed with different deposition current densities: (**a**) 0.63 mA/cm^2, (**b**) 0.83 mA/cm^2 and (**c**) 1.03 mA/cm^2.

Figure 5 shows the effect of the distance between the electrodes (1, 2, 4 and 5 cm) on the uniformity of the activity of the 25.5 cm^2 large area Ag GDE according to the position. The deposition current density and deposition time were fixed at 0.83 mA/cm^2 and 50 min, respectively. The total current density and CO current density for each case according to the position are shown in Figure 5a. The total current density and CO current density exhibited good uniformity, with slight differences of 0.61, 0.29, 0.24 and 0.43 mA/cm^2 in the total current density and 0.36, 0.3, 0.22 and 0.16 mA/cm^2 in the CO current density for distance between working and counter electrodes of 1, 2, 4 and 5 cm, respectively. In general, a shorter distance between the electrodes yielded a larger variation in the CO current density. Figure 5b presents the H$_2$ and CO FE according to the electrode distance. As shown, the CO FE at different positions was 73.15%–83.37% (10.22% difference), 80.36%–86.67% (6.31% difference), 81.95%–85.2% (3.25% difference), and 71.17%–81.43% (10.26% difference) for the distances of 1, 2, 4 and 5 cm, respectively. The highest average CO FE of 83.78% and the smallest CO FE variation of 3.25% were observed for the 4 cm distance. The drop of CO FE in the case of 5 cm is probably due to the voltage loss during the deposition resulting from the increased solution resistance between the electrodes. This implies that there might be a counterbalance between the uniformity in the distribution of the deposition current and the ohmic drops as the electrode distance changes, giving that 4 cm as the most desirable distance under this system.

Figure 6 shows the morphologies of the Ag GDE according to the distance between the electrodes and the position. Likely to the small variation in the total/CO current densities and FE (Figure 5), the morphology and uniformity were similar among the Ag deposits, and all the samples exhibited dendrite morphologies with slight deviation in the dendrite densities.
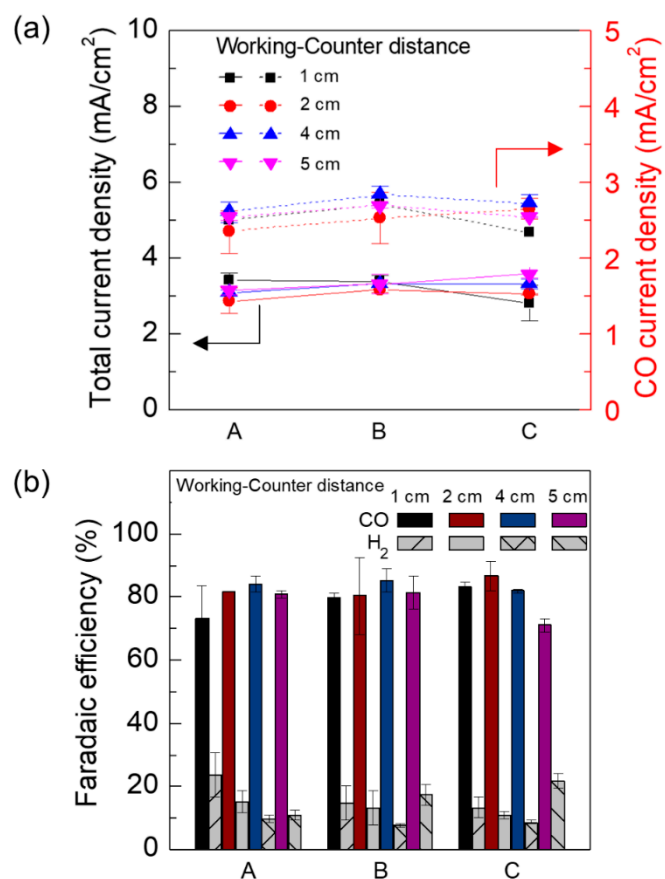
Figure 5. (**a**) Total electrolysis current density and CO production current density of the 25.5 cm^2 Ag GDE according to the position and (**b**) the corresponding FE for CO and H_2. Ag deposition was performed at 0.83 mA/cm^2 for 50 min with different working-counter electrode distances: 1, 2, 4 and 5 cm. The CO_2 reduction was performed at a constant voltage of −1.5 V (vs. SCE) in a laboratory-made H-type cell. 0.5 M $KHCO_3$ was used for both the anolyte and the catholyte.
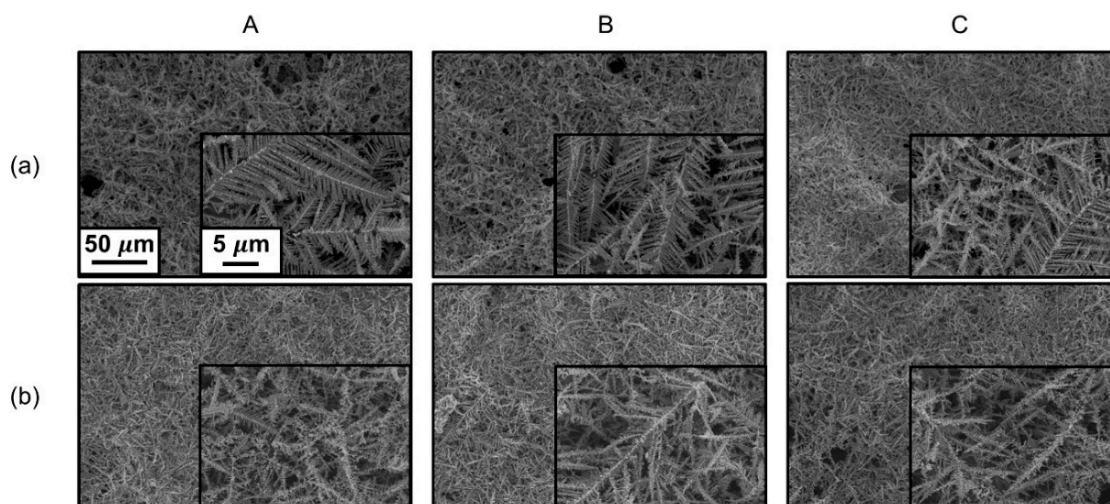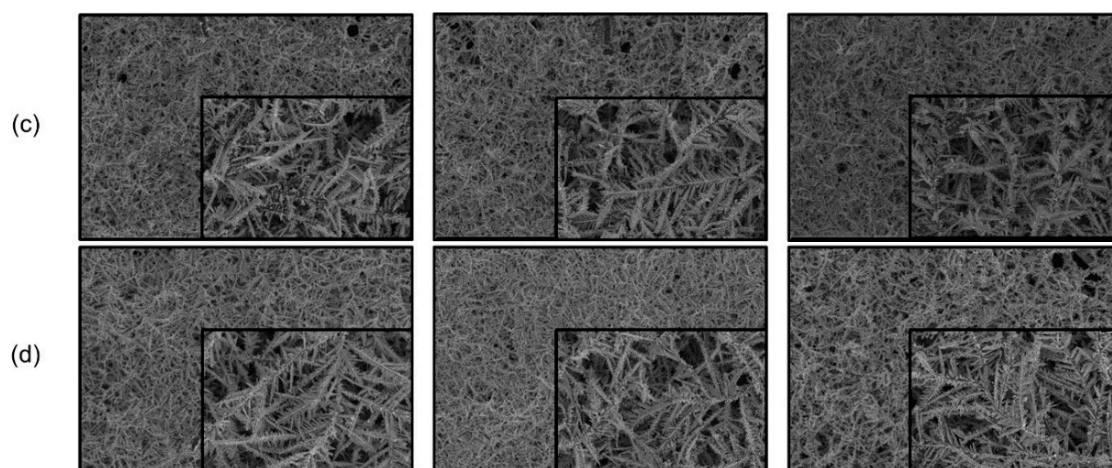

Figure 6. *Cont.*

Figure 6. FE-SEM images of the fabricated 25.5 cm^2 Ag GDE (Figure 5) according to the position on the electrode. Ag deposition was performed with different working–counter electrode distances: (**a**) 1 cm, (**b**) 2 cm, (**c**) 4 cm, and (**d**) 5 cm.

As a final variable, the deposition time was reduced to 5 min with simultaneous variation of the distance between the electrodes, at a fixed deposition current of 0.83 mA/cm^2. Figure 7 shows the total and CO current density, as well as the FE of H$_2$ and CO. In general, the reduction in the deposition time to 5 min severely degraded the activity and uniformity of the Ag GDE. For example, low CO current densities of 0.54–0.75 mA/cm^2 at a 1 cm distance, 0.49–0.64 mA/cm^2 at a 2 cm distance, and 0.62–0.83 mA/cm^2 at a 4 cm distance were observed. Additionally, the calculated CO FE in Figure 7b was relatively low, and exhibited non-uniform behavior with the decrease in the deposition time compared with the 50 min deposition cases in Figure 5, regardless of the electrode distance. The deteriorated activity and uniformity were closely related to the morphology of the Ag GDE, as shown in Figure 8. In contrast to the fully covered deposits in Figure 6 obtained with a longer deposition time of 50 min, the Ag deposits shown in Figure 8 exhibited relatively low coverage, with less-developed short dendrites at the main branches of the carbon paper. These relatively less-developed catalysts are believed to be the cause of the low CO current and non-uniformity. Position A had more dense Ag deposits than the other two positions when the distance between the electrodes was 1 and 2 cm.
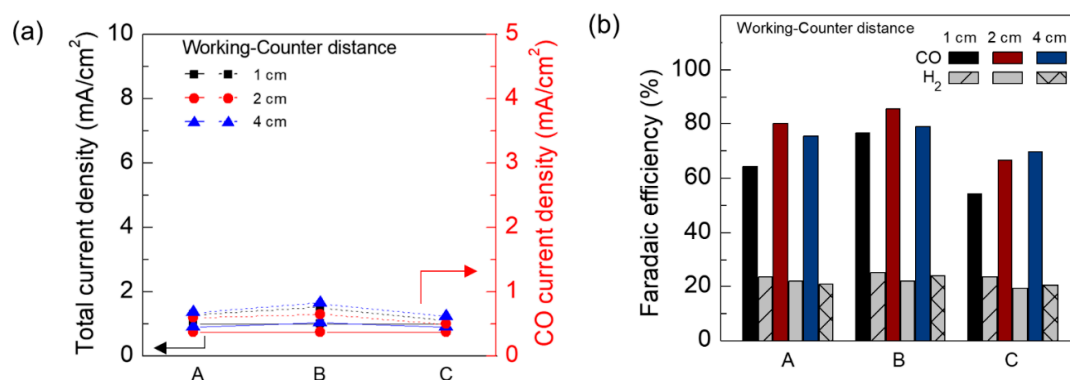

Figure 7. (**a**) Total electrolysis current density and CO production current density of the 25.5 cm^2 Ag GDE according to the position and (**b**) the corresponding FE for CO and H$_2$. Ag deposition was performed at 0.83 mA/cm^2 for 5 min with different working-counter electrode distances: 1, 2 and 4 cm. The CO$_2$ reduction was performed at a constant voltage of −1.5 V (vs. SCE) in a laboratory-made H-type cell. 0.5 M KHCO$_3$ was used for both the anolyte and the catholyte.
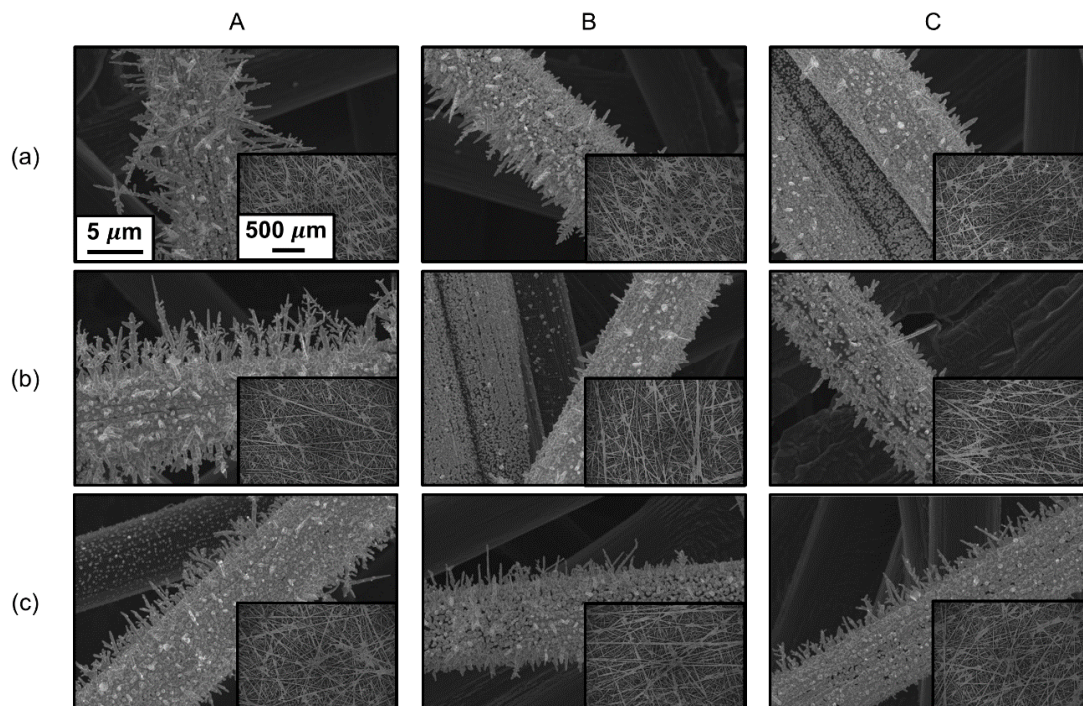
Figure 8. FE-SEM images of the fabricated 25.5 cm^2 Ag GDE (Figure 7) according to the position on the electrode. Ag deposition was performed at 0.83 mA/cm^2 for 5 min with different working-counter electrode distances: (**a**) 1 cm, (**b**) 2 cm, and (**c**) 4 cm.

Using the optimized deposition variables that yielded the highest CO current density, CO FE, and uniformity in the fabrication of the 25.5 cm^2 Ag GDE (two-electrode system, 0.83 mA/cm^2 deposition current, 4 cm working–counter electrode distance, and 50 min deposition time), we fabricated a larger GDE with an area of 136 cm^2. For this larger Ag GDE, five different positions were selected to evaluate the uniformity (Figure 9a). First, the uniformity of the deposit was confirmed using FE-SEM, and the results are shown in Figure 9a. The coverage and morphology of the Ag deposit were not significantly different for the different positions (A–E), and were very similar to those of the 25.5 cm^2 GDE. The total current density, CO current density, and FE of CO/H$_2$ were also evaluated according to the position, and the results are presented in Figure 9b,c. Although the variation of the CO current density among the positions was slightly enhanced with the increased area of 136 cm^2, excellent uniformity in both the total current density and CO FE was observed. The average CO current density among the positions was 2.76 mA/cm^2. The average CO FE was as high as 82.78%. This implies that the optimized deposition variables were successfully employed for the fabrication of a very-large-area Ag GDE with highly uniform CO production activity within the electrode.

Figure 10 shows the performance of MEA-type CO$_2$ electrolyzer with 136 cm^2 Ag GDE (actual geometric area of 107.44 cm^2) according to the cell potential (V_{cell}) ranging from 1.8 to 3.4 V. The loading amounts of Ag were measured by ICPOES to be 1.32 mg/cm^2. Figure 10a exhibits the total reduction current density, giving an increasing trend of the total current density with V_{cell}. At a V_{cell} of 1.8 V, the total current density was very close to 0, implying that almost no reduction reaction was happening. As the V_{cell} was gradually increased, the total current density was substantially increased, giving 151.66 mA/cm^2 at 3.4 V. The produced CO ratio over the other gaseous products (mostly H$_2$; no other gaseous products were detected with GC) was calculated and shown in Figure 10b. Likewise our previous results [36,41], the CO ratio according to the V_{cell} exhibited a peak value of 57.75% at 2.2 V. At lower or higher V_{cell} than 2.2 V, the CO ratio rapidly decreased showing a volcano-like behavior. Particularly at high V_{cell} over 3 V, most of the electrolysis currents came from vigorous hydrogen evolution giving a very low CO ratio. Therefore, the large area (>100 cm^2) Ag-GDE was effectively fabricated by the optimized electrodeposition method, and the MEA-type electrolyzer using it was

successfully used in the CO_2 electroreduction to produce CO at the operation cell potential between 2.2 to 2.6 V.
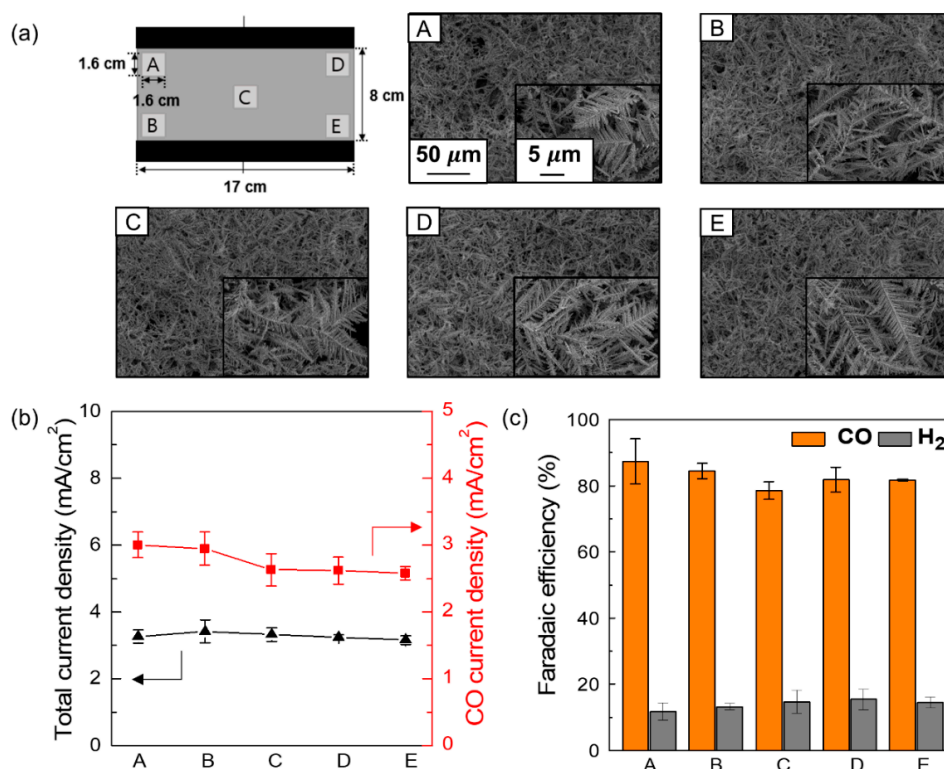

Figure 9. (**a**) FE-SEM images of the fabricated 136 cm^2 Ag GDE according to the position on the electrode. Ag deposition was performed at 0.83 mA/cm^2 for 50 min with a working-counter electrode distance of 4 cm. (**b**) Total electrolysis current density and CO production current density of the 136 cm^2 Ag GDE according to the position and (**c**) the corresponding FE for CO and H_2. The CO_2 reduction was performed at a constant voltage of -1.5 V (vs. SCE) in a laboratory-made H-type cell. 0.5 M $KHCO_3$ was used for both the anolyte and the catholyte.
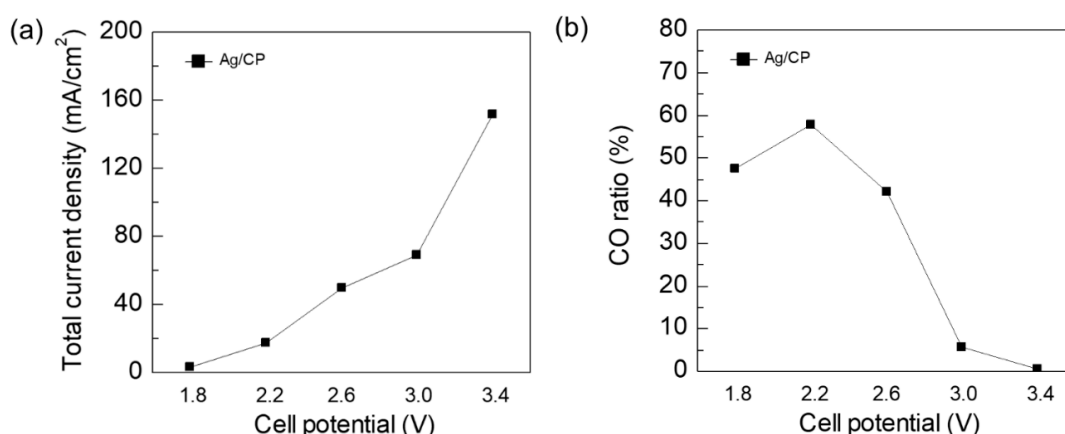

Figure 10. Performance of large area (107.44 cm^2) MEA-type CO_2 electrolyzer according to the applied cell potential (1.8 to 3.4 V) under pressurized condition at 4 bar; (**a**) total reduction current density and (**b**) CO ratio over other gaseous products. The 136 cm^2 large area Ag GDE fabricated by the optimized electrodeposition method (Figure 9) was cut to make 107.44 cm^2 Ag GDE. 10 mL/min of 1.0 M $KHCO_3$ solution and 100 mL/min of 1.0 M KOH solution were fed and circulated as the catholyte and anolyte, respectively, using flow fields at both electrodes. Gaseous CO_2 at a rate of 150 mL/min were also fed to the cathode using a separated flow field.

4. Conclusions

The electrodeposition variables were optimized for fabricating large area (25.5 and 136 cm^2) Ag GDEs for application to an MEA-type CO_2 electrolyzer. In the fabrication of a large electrode via electrodeposition, it is essential to achieve uniformity among different positions on the electrode, which requires optimization of the electrode system, electrode arrangement, deposition current, and deposition time. By comparing the total electrolysis current, CO production current, FE and deposition morphology, it was confirmed that galvanostatic deposition at 0.83 mA/cm^2 for 50 min in a horizontal two-electrode system with a working-counter electrode distance of 4 cm was the best condition for fabricating the large area Ag GDE with uniform performance throughout the electrode. Position-averaged CO current densities of 2.72 and 2.76 mA/cm^2 and FEs of 83.78% and 82.78% were obtained for 25.5 and 136 cm^2 Ag GDEs, respectively. The fabricated large area Ag GDE (actual geometric area of 107.44 cm^2) was be used in MEA-type CO_2 electrolyzers, giving potential-dependent CO conversion efficiencies of 41.99%–57.75% at V_{cell} = 2.2–2.6 V.

Author Contributions: Conceptualization, S.-K.K.; Formal analysis, S.-K.K. and J.H.J.; Funding acquisition, S.-K.K.; Investigation, S.O., H.P., H.K., Y.S.P. and M.G.H.; Methodology, S.O. and S.-K.K.; Supervision, S.-K.K.; Validation, S.-K.K. and J.H.J.; Writing—original draft, S.O. and H.P.; Writing—review and editing, S.-K.K. All authors have read and agreed to the published version of the manuscript.

Conflicts of Interest: The authors declare no conflict of interest.

References

1. Appel, A.M.; Bercaw, J.E.; Bocarsly, A.B.; Dobbek, H.; DuBois, D.L.; Dupuis, M.; Ferry, J.G.; Fujita, E.; Hille, R.; Kenis, P.J.A.; et al. Frontiers, Opportunities, and Challenges in Biochemical and Chemical Catalysis of CO_2 Fixation. *Chem. Rev.* **2013**, *113*, 6621–6658. [CrossRef] [PubMed]
2. Kumar, B.; Llorente, M.; Froehlich, J.; Dang, T.; Sathrum, A.; Kubiak, C.P. Photochemical and Photoelectrochemical Reduction of CO_2. *Annu. Rev. Phys. Chem.* **2012**, *63*, 541–569. [CrossRef] [PubMed]
3. Mikkelsen, M.; Jorgensen, M.; Krebs, F.C. The teraton challenge. A review of fixation and transformation of carbon dioxide. *Energy Environ. Sci.* **2010**, *3*, 43–81. [CrossRef]
4. Mendoza, J.A.; Kim, H.K.; Park, H.K.; Park, K.Y. Photocatalytic reduction of carbon dioxide using Co_3O_4 nanoparticles under visible light irradiation. *Korean J. Chem. Eng.* **2012**, *29*, 1483–1486. [CrossRef]
5. Wang, W.; Wang, S.P.; Ma, X.B.; Gong, J.L. Recent advances in catalytic hydrogenation of carbon dioxide. *Chem. Soc. Rev.* **2011**, *40*, 3703–3727. [CrossRef]
6. Whipple, D.T.; Kenis, P.J.A. Prospects of CO_2 Utilization via Direct Heterogeneous Electrochemical Reduction. *J. Phys. Chem. Lett.* **2010**, *1*, 3451–3458. [CrossRef]
7. Hori, Y. *Electrochemical CO_2 Reduction on Metal Electrodes*; Springer: New York, NY, USA, 2008; Volume 42, pp. 89–189.
8. Singh, M.R.; Kwon, Y.; Lum, Y.; Ager, J.W.; Bell, A.T. Hydrolysis of Electrolyte Cations Enhances the Electrochemical Reduction of CO_2 over Ag and Cu. *ACS Catal.* **2016**, *138*, 13006–13012. [CrossRef]
9. Sun, K.; Wu, L.; Qin, W.; Zhou, J.; Hu, Y.; Jiang, Z.; Shen, B.; Wang, Z. Enhanced electrochemical reduction of CO_2 to CO on Ag electrocatalysts with increased unoccupied density of states. *J. Mater. Chem. A* **2016**, *4*, 12616–12623. [CrossRef]
10. Hirunsit, P.; Soodsawang, W.; Limtrakul, J. CO_2 Electrochemical Reduction to Methane and Methanol on Copper-Based Alloys: Theoretical Insight. *J. Phys. Chem. C* **2015**, *119*, 8238–8249. [CrossRef]
11. Peterson, A.A.; Norskov, J.K. Activity Descriptors for CO_2 electroreduction to Methane on Transition-Metal Catalysts. *J. Phys. Chem. Lett.* **2012**, *3*, 251–258. [CrossRef]
12. Chen, C.S.; Wan, J.H.; Yeo, B.S. Electrochemical Reduction of Carbon Dioxide to Ethane Using Nanostructured Cu_2O-Derived Copper Catalyst and Palladium(II) Chloride. *J. Phys. Chem. C* **2015**, *119*, 26875–26882. [CrossRef]

13. Yang, K.D.; Ko, W.R.; Lee, J.H.; Kim, S.J.; Lee, H.; Lee, M.H. Morphology-Directed Selective Production of Ethylene of Ethane from CO_2 on a Cu Mesopore Electrode. *Angew. Chem. Int. Ed.* **2016**, *56*, 796–800. [CrossRef] [PubMed]

14. Kortlever, R.; Peters, I.; Koper, S.; Kopr, T.M. Electrochemical CO_2 reduction to Formic Acid at Low Overpotential and with High Faradaic Efficiency on Carbon-Supported Bimetallic Pd-Pt Nanoparticles. *ACS Catal.* **2015**, *5*, 3916–3923. [CrossRef]

15. Alvarex-Guerra, M.; Quintanilla, S.; Irabien, A. Conversion of carbon dioxide into formate using a continuous electrochemical reduction process in a lead cathode. *Chem. Eng. J.* **2012**, *207–208*, 278–284. [CrossRef]

16. Peterson, A.A.; Abild-Pedersen, F.; Studt, F.; Rossmeisl, J.; Norskov, J.K. How copper catalyzes the electroreduction of carbon dioxide into hydrocarbon fuels. *Energy Environ. Sci.* **2010**, *3*, 1311–1315. [CrossRef]

17. Oh, W.; Rhee, C.K.; Han, J.W.; Shong, B. Atomic and Molecular Adsorption on the Bi(111) Surface: Insights into Catalytic CO_2 Reduction. *J. Phys. Chem. C* **2018**, *122*, 23084–23090. [CrossRef]

18. Li, W. *Electrocatalytic Reduction of CO_2 to Small Organic Molecule Fuels on Metal Catalysts*; ACS Publications: Washington, DC, USA, 2010; pp. 55–76.

19. Keim, W. Carbon monoxide: Feedstock for chemicals, present and future. *J. Organomet. Chem.* **1989**, *372*, 15–23. [CrossRef]

20. Kuhl, K.P.; Hatsukade, T.; Cave, E.R.; Abram, D.N.; Kibsgaard, J.; Jaramillo, T.F. Electrocatalytic Conversion of Carbon Dioxide to Methane and Methanol on Transition Metal Surfaces. *J. Am. Chem. Soc.* **2014**, *136*, 14107–14113. [CrossRef]

21. Katayama, Y.; Nattino, F.; Giordano, L.; Hwang, J.; Rao, R.R.; Andreussi, O.; Marzari, N.; Shao-Horn, Y. An In Situ Surface-Enhanced Infrared Absorption Spectroscopy Study of Electrochemical CO_2 Reduction: Selectivity Dependence on Surface C-Bound and O-Bound Reaction Intermediates. *J. Phys. Chem. C* **2019**, *123*, 5951–5963. [CrossRef]

22. Kim, C.; Jeon, H.S.; Eom, T.; Jee, M.S.; Kim, H.; Friend, C.M.; Min, B.K.; Hwang, Y.J. Achieving Selective and Efficient Electrocatalytic Activity for CO_2 Reduction Using Immobilized Silver Nanoparticles. *J. Am. Chem. Soc.* **2015**, *137*, 13844–13850. [CrossRef]

23. Hsieh, Y.C.; Senanayake, S.D.; Wenqian, Y.Z.; Xu, W.; Polyansky, D.E. Effect of Chloride Anions on the Synthesis and Enhanced Catalytic Activity of Silver Nanocoral Electrodes for CO_2 Electroreduction. *ACS Catal.* **2015**, *5*, 5349–5356. [CrossRef]

24. Liu, S.; Tao, H.; Zeng, L.; Liu, Q.; Xu, Z.; Liu, Q.; Luo, J.-L. Shape-Dependent Electrocatalytic Reduction of CO_2 to CO on Triangular Silver Nanoplates. *J. Am. Chem. Soc.* **2017**, *139*, 2160–2163. [CrossRef] [PubMed]

25. Back, S.; Yeom, M.S.; Jung, Y. Active Sites of Au and Ag Nanoparticle Catalysts for CO_2 Electroreduction to CO. *ACS Catal.* **2015**, *5*, 5089–5096. [CrossRef]

26. Tornow, C.E.; Thorson, M.R.; Ma, S.; Gewirth, A.A.; Kenis, P.J.A. Nitrogen-Based Catalysts for the Electrochemical Reduction of CO_2 to CO. *J. Am. Chem. Soc.* **2012**, *134*, 19520–19523. [CrossRef]

27. Rosen, J.; Hutchings, G.S.; Lu, Q.; Forest, R.V.; Moore, A.; Jiao, F. Electrodeposited Zn Dendrites with Enhanced CO Selectivity for Electrocatalytic CO_2 Reduction. *ACS Catal.* **2015**, *5*, 4586–4591. [CrossRef]

28. Zhu, W.; Michalsky, R.; Metin, O.; Lv, H.; Guo, S.; Wright, C.J.; Sun, X.; Peterson, A.A.; Sun, S. Monodisperse Au Nanoparticles for Selective Electrocatalytic Reduction of CO_2 to CO. *J. Am. Chem. Soc.* **2013**, *135*, 16833–16836. [CrossRef]

29. Luc, W.; Collins, C.; Wang, S.; Xin, H.; He, K.; Kang, Y.; Jiao, F. Ag-Sn Bimetallic Catalyst with a Core-Shell Structure for CO_2 Reduction. *J. Am. Chem. Soc.* **2017**, *139*, 1885–1893. [CrossRef]

30. Duan, Z.; Sun, R. Am improved model calculating CO_2 solubility in pure water and aqueous NaCl solutions from 273 to 533 K and from 0 to 2000 bar. *Chem. Geol.* **2003**, *193*, 257–271. [CrossRef]

31. Dufek, E.J.; Lister, T.E.; Stone, S.G.; Mcllwain, M.E. Operation of a pressurized system for continuous reduction of CO_2. *J. Electrochem. Soc.* **2012**, *159*, F514–F517. [CrossRef]

32. Dufek, E.J.; Lister, T.E.; Mcllwain, M.E. Influence of S Contamination on CO_2 Reduction at Ag Electrodes. *J. Electrochem. Soc.* **2011**, *158*, B1384–B1390. [CrossRef]

33. Kim, B.; Ma, S.; Jhong, H.-R.M.; Kenis, J.A. Influence of dilute feed and pH on electrochemical reduction of CO_2 to CO on Ag in a continuous flow electrolyzer. *Electrochim. Acta* **2015**, *166*, 271–276. [CrossRef]

34. Delacourt, C.; Ridgway, P.L.; Kerr, J.B.; Newman, J. Design of an Electrochemical Cell Making Syngas ($CO + H_2$) from CO_2 and H_2O Reduction at Room Temperature. *J. Electrochem. Soc.* **2008**, *155*, B42–B49. [CrossRef]

35. Wu, J.; Risalvato, F.G.; Sharma, P.P.; Pellechia, P.J.; Ke, F.S.; Zhou, X.D. Electrochemical Reduction of Carbon Dioxide II. Design, Assembly, and Performance of Low Temperature Full Electrochemical Cells. *J. Electrochem. Soc.* **2013**, *160*, F953–F957. [CrossRef]

36. Ham, Y.S.; Park, Y.S.; Jo, A.; Jang, J.H.; Kim, S.-K.; Kim, J.J. Proton-exchange membrane CO_2 electrolyzer for CO production using Ag catalyst directly electrodeposited onto gas diffusion layer. *J. Power Sources* **2019**, *437*, 226898. [CrossRef]

37. Echendu, O.K.; Okeoma, K.B.; Oriaku, C.I.; Dharmadasa, I.M. Electrochemical Deposition of CdTe Semiconductor Thin Films for Solar Cell Application Using Two-Electrode and Three-Electrode Configurations: A Comparative study. *Adv. Mater. Sci. Eng.* **2016**, *2016*, 1–8. [CrossRef]

38. Rajkumar, S.R.; Alagar, M.; Kanagasabapathy, M. Current Density Distribution Studies in Manifold Dimensions. *J. Chem. Pharm. Res.* **2012**, *4*, 1173–1178.

39. Park, H.; Choi, J.; Kim, H.; Hwang, E.; Ha, D.-H.; Ahn, S.H.; Kim, S.-K. AgIn dendrite catalysts for electrochemical reduction of CO_2 to CO. *Appl. Catal. B* **2017**, *219*, 123–131. [CrossRef]

40. Ham, Y.S.; Choe, S.; Kim, M.J.; Lim, T.; Kim, S.-K.; Kim, J.J. Electrodeposited Ag catalysts for the electrochemical reduction of CO_2 to CO. *Appl. Catal. B* **2017**, *208*, 35–43. [CrossRef]

41. Oh, S.; Park, Y.S.; Park, H.; Kim, H.; Jang, J.H.; Choi, I.; Kim, S.-K. Ag-deposited Ti gas diffusion electrode in proton exchange membrane CO_2 electrolyzer for CO production. *J. Ind. Eng. Chem.* **2020**, *82*, 374–382. [CrossRef]

42. Choi, J.; Kim, M.J.; Ahn, S.H.; Choi, I.; Jang, J.H.; Ham, Y.S.; Kim, J.J.; Kim, S.-K. Electrochemical CO_2 reduction to CO on dendritic Ag-Cu electrocatalysts prepared by electrodeposition. *Chem. Eng. J.* **2016**, *299*, 37–44. [CrossRef]